available at www.sciencedirect.com

ScienceDirect

journal homepage: www.elsevier.com/locate/agrformet

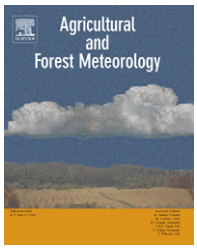

Evaluation of land surface radiation balance derived from moderate resolution imaging spectroradiometer (MODIS) over complex terrain and heterogeneous landscape on clear sky days

Youngryel Ryu [a,1], *Sinkyu Kang* [b,*], *Sang-Ki Moon* [c], *Joon Kim* [c]

[a] *Department of Environmental Planning, Graduate School of Environmental Studies, Seoul National University, San 56-1, Sillim-dong, Gwanak-gu, Seoul 151-742, Republic of Korea*
[b] *Department of Environmental Science, Kangwon National University, Chunchon 200-701, Republic of Korea*
[c] *Global Environment Laboratory & Department of Atmospheric Sciences, Yonsei University 134, Sinchon-dong, Seodaemun-gu, Seoul 120-749, Republic of Korea*

ARTICLE INFO

Article history:
Received 7 June 2007
Received in revised form
29 April 2008
Accepted 9 May 2008

Keywords:
MODIS
Terra
Aqua
Net radiation
Heterogeneity
Complex terrain
KoFlux

ABSTRACT

Many studies on land surface radiation balances have relied on geostationary satellites. These satellites have provided data with high temporal resolution (less than 3 h); however, the spatial resolution was too coarse (20–250 km scale) to investigate local-scale land surface radiation balances. Moderate resolution imaging spectroradiometer (MODIS) – onboard both the Terra and Aqua satellites – yields a tradeoff with regard to this problem by providing higher spatial resolution (~1 km scale) and sensing all over the earth nearly twice a day during daytime; this provides a potential tool for the periodical monitoring of the land surface energy balance. The reliability of MODIS-derived estimates is, however, affected by the presence of multiple error sources, such as those related to heterogeneous land cover and complex topography. In this study, we have used atmospheric (5 and 10 km scale) and land (1 km scale) products obtained from both the Terra and Aqua MODIS devices as inputs in order to estimate the radiation components (1 km scale) under clear daytime conditions over a heterogeneous farmland area and a rugged deciduous forest in the Korea Flux Network (KoFlux). The reliability of these estimates and the associated errors were evaluated by comparing against field measurements taken for 41 and 26 clear days with regard to the farmland and forest sites, respectively. Solar radiation was successfully retrieved with a root mean square error (RMSE) of ~20 W m^{-2} for both the Terra and Aqua devices over the flat farmland site, whereas the rugged forest site exhibited corresponding values of 40 and 65 W m^{-2} RMSE values with consistent positive biases (presumably caused by topographic effects). The RMSE values of the downward longwave radiation were ~20 W m^{-2} for both the Terra and Aqua devices for both these sites. The sensitivities of the upward components of the shortwave and longwave radiations varied with the RMSE values to the scale of the spatial heterogeneity of both the sites. Consequently, the RMSE values of the net radiation ranged from 33 to 61 W m^{-2} for both the devices at both the sites. Our results suggest that

* *Corresponding author*. Tel.: +82 33 250 8578; fax: +82 250 251 3991.
E-mail address: kangsk@kangwon.ac.kr (S. Kang).
[1] Present address: Ecosystem Sciences Division, Department of Environmental Science, Policy and Management, University of California, Berkeley, CA 94720-3114, USA.
0168-1923/$ – see front matter
doi:10.1016/j.agrformet.2008.05.008

the scales of the patch mosaics within the landscapes need to be quantified for proper retrieval of the MODIS-derived radiation products. More extensive validation efforts are required to identify and account for major error sources across diverse land surface conditions.

1. Introduction

Net radiation (R_n) is the balance between the upwelling and downwelling streams of shortwave (R_s) and longwave (R_l) radiation, which is the fundamental quantity of energy budget at the earth's surface. The partitioning of R_n into evapotranspiration (E) and other energy budget components is firmly coupled with changes in land use and global climate conditions. Most E models require R_n as the core input parameter (Boegh et al., 2002; Monteith, 1965; Nishida et al., 2003; Priestley and Taylor, 1972; Shuttleworth and Wallace, 1985; Su, 2002), and an accurate estimation of R_n is essential for regional water resource management.

Many studies on land surface radiation balances have relied on geostationary satellites, which are essential in providing data with fine temporal resolution (less than 3 h) and coarse spatial resolutions of 20–250 km scale (Gautier et al., 1980; Harries et al., 2005; Jacobs et al., 2002; Pinker and Laszlo, 1992; Zhang et al., 2004). R_n schemes derived entirely using remote sensing at moderate resolution scales are rare. For a scale of less than 1 km, several studies have relied on the field measurements of solar radiation (Boegh et al., 2002) or forcing data for calculating solar radiation (Dubayah, 1992; Gratton et al., 1993; Ma, 2003) and on meteorological modeling data (Su et al., 2005). MODIS compromises on the spatiotemporal scale issue of geostationary satellites (i.e., four times per day with a resolution of ~1 km scale). Further, it provides detailed atmospheric and land surface properties, which yield the R_n schemes entirely derived from MODIS; this reduces the error sources arising from different sensor architectures.

Terra and Aqua satellites have onboard MODIS sensors that yield regular and frequent observations of biophysical variables with moderate resolution (~1 km) and that cover the entire globe. The MODIS science team provides 4 disciplines (namely, land, atmosphere, ocean, and calibration) with 40 sub-products in support of 36 spectral bands spanning the visible, near-infrared, and thermal regions of the electromagnetic spectrum. Diverse products and spectral bands enable scientists to more accurately estimate the land surface energy budgets (Bisht et al., 2005; Houborg and Soegaard, 2004; Kustas et al., 2003; Nishida et al., 2003). Terra rotates in a descending orbit with its equatorial crossing time at 10:30 a.m. when the cloud cover is less; on the other hand, Aqua crosses the equator in an ascending orbit at 1:30 p.m. focusing on clouds, precipitation, and other meteorological phenomena (Masuoka et al., 1998). These two MODIS platforms in complementary orbits may yield information on diurnal variations in the biophysical variables of land, atmosphere, and ocean, four times per day (Justice et al., 1998, 2002; Masuoka et al., 1998). In combination with the National Polar Operational Environmental Satellite System (NPOESS) and NPOESS Preparatory Project (NPP) to be launched in the near future (Townshend and Justice, 2002), Terra and Aqua MODIS sensors would enable us to better understand the diurnal variations in the land surface processes with finer spatial resolution as compared to those obtained using geostationary satellites. The utilization of MODIS images for detecting diurnal variations, however, has not been adequately tested. A few studies have examined the diurnal variations in MODIS-derived land surface temperatures (LST) (Wan et al., 2004; Zhang et al., 2005).

Spatial heterogeneity and complexity of land covers are the most challenging features in land surface modeling and satellite remote sensing of biophysical variables (Baldocchi et al., 2005; Kustas and Norman, 2000; Li and Avissar, 1994). Many researchers have investigated the effect of land surface heterogeneity with regard to albedo (Jin et al., 2003; Salomon et al., 2006), LST (Brunsell and Gillies, 2003; Jacob et al., 2004; Lakshmi and Zehrfuhs, 2002; Liu et al., 2006; Moran et al., 1997), and land surface emissivity (Pu et al., 2006; Wan et al., 2002). Jin et al. (2003), for example, tested the effect of land surface heterogeneity on the MODIS albedo; they reported small errors in the growing season with lush vegetation but greater errors during fall and winter. However, if the sub-grid variability within a pixel is significant in the growing season, this argument would be invalid. Bisht et al. (2005) proposed a R_n scheme entirely derived from MODIS without validating the individual components of the radiation budget, which are vulnerable to error sources induced by land surface heterogeneity.

In this study, we tested the reliability of the MODIS-derived biophysical variables over two contrasting landscapes: (1) a farmland site with heterogeneous land cover over flat topography and (2) a forest site with patchy land cover over complex topography. Our objectives included the validation of the MODIS-derived surface radiation components and the analysis of their error sources related to landscape heterogeneity. First, we validated the MODIS-derived biophysical variables (namely, air temperature, vapor pressure, and albedo) that were used as the inputs for radiation estimation. Then, we estimated the MODIS-derived radiation components and associated errors by comparing against field measurements. Further, we examined the Landsat ETM+ images of the two sites using semivariogram analysis and quantified the scale of heterogeneity of the LST and albedo. In our final discussion, we address the error sources and the effect of varying the scales of heterogeneity within a pixel on the MODIS-derived radiation estimates.

2. Materials and methods

2.1. Study sites and field measurements

The study sites include a deciduous forest in the Gwangneung Experimental Forest (GEF) and a farmland in Haenam in the

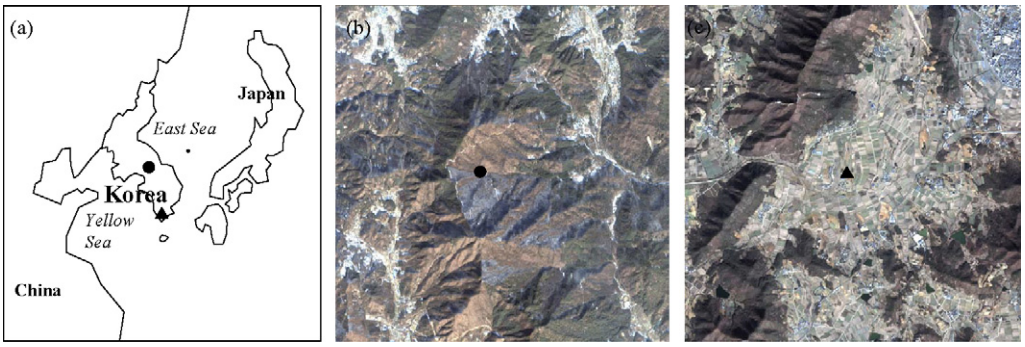

Fig. 1 – Study sites: (a) location of Gwangneung deciduous forest (DK, black-filled circle) and Haenam farmland (FK, black-filled triangle) study sites; (b) IKONOS image of an 5 km × 5 km area around DK site; (c) IKONOS image of a 5 km × 5 km area over the FK site.

Korea Flux Network (Kim et al., 2006b) (Fig. 1). The deciduous forest site (DK) in GEF is located in the midwestern part of the Korean Peninsula (37.7487°N, 127.1489°E); it belongs to a typical cool-temperate broadleaved forest zone with complex terrain. It covers an area of 21.7 km^2, and the elevation ranges from 270 to 490 m. The DK site is dominated by *Quercus acutissima*, *Quercus serrata*, *Carpinus laxiflora*, and *Acer palmatum*, and the overstory canopy height is approximately 18 m. The annual maximum, minimum, and mean temperatures are 35, −15, and 10 °C, respectively. The annual mean precipitation is 1365 mm (Lim et al., 2003). The flux tower measurements have been acquired since 2000. In this study, we used the data from May 1 to December 31, 2002 (i.e., from day 122 to day 365 of the year). The radiation components were measured at a height of 40 m above the ground by using a Kipp and Zonen CNR-1 radiometer (Kipp and Zonen, The Netherlands), while the air temperature T_a and vapor pressure e_0 were measured at a height of 30 m above the ground by using Vaisala HMP-35 Humicap (Vaisala, Finland). Both sets of measurements were acquired at intervals of 30 min in averages (Choi et al., 2005).

The farmland site in Haenam (FK) is located in the southwestern corner of the Korean Peninsula (34.5539°N, 126.5697°E). The land cover within a 300 m radius of the flux tower mainly comprises cultivated crops, including beans, sweet potatoes, Indian millet, and sesame; there are rice paddies to the south and west of the tower. Beyond this region, rice paddies prevail along the south and west. In addition, scattered residential areas, roads, and isolated forests coexist. The nearest forest is located approximately 800 m to the north of the flux tower. The dominant canopy height is approximately 1 m. The annual maximum, minimum, and mean temperatures are 32, −12, and 13 °C, respectively. The annual mean precipitation is 1306 mm (Lee et al., 2003). The tower flux measurements were acquired since 2002. In this study, we used the data from October 2002 to September 2003. The radiation components were measured at a height of 10.5 m above the ground by using a Kipp and Zonen CNR-1 radiometer (Kipp and Zonen, The Netherlands), while T_a and e_0 were measured at a height of 20 m above the ground by using an eddy covariance system (CSAT3 sonic anemometer, Campbell Scientific, Logan, UT, USA & LI7500 CO2/H20 gas analyzer, LI-COR, NE, USA). The flux tower observations were linearly interpolated to coincide with the overpassing times of the Terra and Aqua satellites. The instantaneous imaging time for each pixel was obtained from the hierarchical data format (HDF) files. In this study, only the daytime MODIS data were used because we focus on the validation of the MODIS-derived solar radiation scheme.

2.2. Retrieval of net radiation from MODIS

Net radiation, R_n, at the land surface can be expressed as

$$R_n = R_s\downarrow - R_s\uparrow + R_l\downarrow - R_l\uparrow \quad (1)$$

where R_s and R_l denote the shortwave and longwave radiations and ↑ and ↓ denote the upwelling and downwelling streams, respectively.

Bisht et al. (2005) proposed a methodology for estimating R_n derived entirely from MODIS. We employed a similar approach, except for our analysis of solar radiation, albedo, and land surface emissivity. For selecting the datasets for days with clear skies, we examined the fifth byte of the quality assurance bit field (i.e., the number of 1 km^2 clear pixels within a 25 km^2 pixel) in MOD/MYD07 (atmospheric profile product), and selected the data for perfectly clear days (i.e., the number of clear pixels is 25). We used various spatiotemporal MODIS products (Table 1), assuming that all the products are homogeneous in the sub-pixel scale over the period. The schematic diagram to estimate R_n is shown in Fig. 2, and detailed explanations are provided below.

2.2.1. Downward shortwave radiation

We used the parameterization scheme of $R_s\downarrow$ considering both diffuse and direct beam radiation (Bird and Hulstrom, 1981). This scheme has been accurately evaluated in several studies (Annear and Wells, 2007; Houborg et al., 2007; Houborg and Soegaard, 2004). Direct solar radiation (I_{dir}) can be expressed as

$$I_{dir} = I_0(\cos z)(0.9662)T_R T_O T_{UM} T_W T_A \quad (2)$$

where I_0 is the extraterrestrial solar radiation corrected for the earth–sun distance, z is the solar zenith angle, T_R is the transmittance of Rayleigh scattering, T_O is the transmittance of ozone absorptance, T_{UM} is the transmittance of absorptance of uniformly mixed gases (carbon dioxide and oxygen), T_W is

Table 1 – Spatial and temporal resolution of MODIS products used in this study

MODIS products	Time	Space
MOD/MYD03	5 min	1 km × 1 km
MOD/MYD04	5 min	10 km × 10 km
MOD/MYD05	5 min	5 km × 5 km
MOD/MYD07	5 min	5 km × 5 km
MOD/MYD11A1	5 min	1 km × 1 km
MOD43B3	16 day	1 km × 1 km

MOD and MYD indicate Terra and Aqua, respectively.

the transmittance of water vapor absorption and T_A is the transmittance of aerosol absorptance and scattering. Diffuse radiation (I_{dif}) can be expressed as

$$I_{dif} = I_0(\cos z)(0.79)T_O T_W T_{UM} T_{AA} \frac{0.5(1-T_R)+B_a(1-T_{AS})}{1-M+M^{1.02}} \quad (3)$$

where T_{AA} is the transmittance of aerosol absorptance, B_a is the ratio of the forward-scattered radiation to the total scattered radiation due to aerosols, T_{AS} is the transmittance of aerosol scattering, and M is the air mass. Then, the total downward solar radiation ($R_s\downarrow$) can be expressed as

$$R_s\downarrow = \frac{I_d + I_{as}}{1-\alpha r_s} \quad (4)$$

where α denotes the ground albedo and r_s denotes the atmospheric albedo. The specific parameterization schemes for individual sub-terms can be found in Bird and Hulstrom (1981) and the required parameters can be retrieved from various MODIS atmosphere and land products (Fig. 2).

2.2.2. *Upward shortwave radiation*

The upward shortwave radiation $R_s\uparrow$ can be expressed as

$$R_s\uparrow = \alpha R_s\downarrow \quad (5)$$

White-sky (completely diffuse bihemispherical) albedo and black-sky (completely direct beam directional hemispherical) albedo at the local solar noon are derived from the MODIS solar reflective bands. The albedo products use kernels in a linear bidirectional reflectance distribution function (BRDF) model (Lucht et al., 2000; Schaaf et al., 2002). There are two versions of the MODIS albedo: Terra-derived albedo (MOD43) and Terra-Aqua-integrated albedo (MCD43). High-quality albedo estimations obtained from the latter were only slightly different as compared to those obtained from MOD43 (Salomon et al., 2006); however, the MCD43 observations were not retrieved from January to April in 2003 for the sites under investigation. We, therefore, selected MOD43B3, 16-day and 1 km globally tiled albedo consisting of black- and white-sky albedos for seven spectral bands (band 1–7) and three broadband ranges (0.40–0.70, 0.70–4.0, and 0.25–4.0 μm). The actual albedo (α_a) was calculated using a lookup table (LUT) for the fraction of the diffuse light concerning the solar zenith angle, optical depth, bands, and aerosol model types at the MODIS BRDF home page (http://www-modis.bu.edu/brdf/userguide/tools.html) as

$$\alpha_a(z,b,\text{od},\text{amt}) = \alpha_w(b) \times f_{dif}(z,b,\text{od},\text{amt}) + \alpha_b(z,b) \times (1 - f_{dif}(z,b,\text{od},\text{amt})) \quad (6)$$

where α_w represents the white-sky albedo, α_b the black-sky albedo, f_{dif} the fraction of diffuse light, b the band, od the optical depth at 0.55 μm and amt represents the type of aerosol model. The LUT provides the value of b for the broadband range of 0.25–4.0 μm. In this study, the required input variables in Eq. (6) were fully derived from MODIS such as z from MOD/MYD03 (geolocation product), α_w and α_b from MOD/MYD43, and od from MOD/MYD04 (aerosol product). The measured albedos at the Terra overpass time were averaged over 16 days in accordance with the MODIS albedo product.

2.2.3. *Downward longwave radiation*

The downward longwave radiation ($R_l\downarrow$) can be calculated as

$$R_l\downarrow = \sigma\varepsilon_a T_a^4 \quad (7)$$

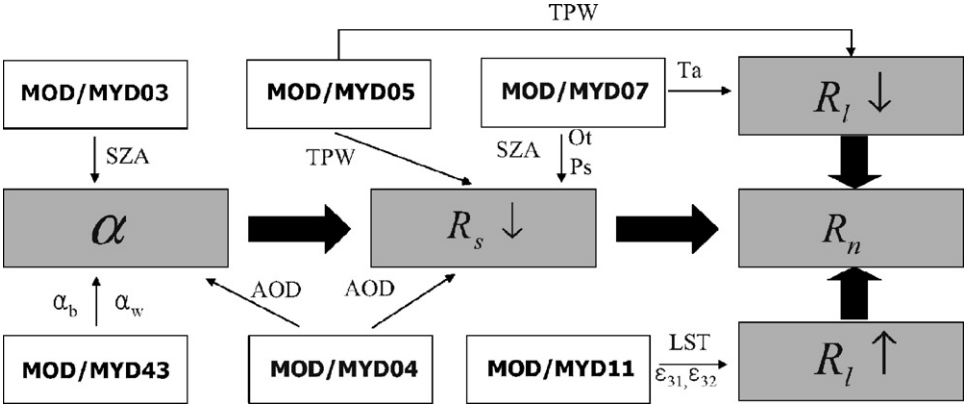

Fig. 2 – Schematic diagram for estimating net radiation (α: albedo, $R_s\downarrow$: downward shortwave radiation, $R_l\downarrow$: downward longwave radiation, $R_l\uparrow$: upward longwave radiation, R_n: net radiation, SZA: solar zenith angle, α_b: black sky albedo, α_w: white sky albedo, AOD: aerosol optical depth, TPW: total column precipitable water, Ot: total ozone, Ps: surface pressure, Ta: air temperature, LST: land surface temperature, ε_{31}: emissivity in band 31, ε_{32}: emissivity in band 32). MOD (MYD) indicates Terra (Aqua), and the numbers (i.e., 3, 4, 5, 7, 11, 43) indicates geolocation, aerosol, water vapor, atmospheric profile, land surface temperature, and albedo products, respectively.

where σ is the Steffan–Boltzmann constant ($5.67 \times 10^{-8}\,W\,m^{-2}\,K^{-4}$), T_a is the air temperature (Kelvin) at the screen level and ε_a is the emissivity of air.

Among the well-known ε_a schemes, we used the scheme proposed by Prata (1996), which was the most accurate among the available schemes (Diak et al., 2004; Kjaersgaard et al., 2007). The scheme estimates the ε_a value for clear-sky days and stable atmospheric conditions as

$$\varepsilon_a = [1 - (1+\xi)\exp\{-(1.2+3\xi)^{0.5}\}] \tag{8}$$

where $\xi = m(e_a/T_a)$. The coefficient m was originally proposed as 46.5 as a globally optimized value. For improving the accuracy, it was recommended that this value be calibrated at the local scale (Prata, 1996). Consequently, it was calculated using nonlinear regression fitting for the DK and FK sites: the calibrated values were 69.7 and 14.8, respectively. We compared the results obtained from using the globally optimized value (46.5) and locally fitted values (69.7 and 14.8) in Section 4.

MOD/MYD07 provides the air and dew-point temperature at 20 different atmospheric pressure levels, employing statistical retrieval with an option for subsequent nonlinear physical retrieval (Seemann et al., 2003). We used these temperature values at a vertical pressure level of 1000 hPa as a surrogate for the screen level (Bisht et al., 2005; Houborg and Soegaard, 2004). The dew-point temperature (T_d) was converted to the actual vapor pressure by using the formula (Monteith and Unsworth, 1990)

$$e_a = e_s(T_d) = 6.11\exp\left\{\frac{19.59(T_d - 273.3)}{T_d}\right\} \tag{9}$$

where $e_s(T_d)$ is the saturated water vapor pressure at T_d.

2.2.4. *Upward longwave radiation*

The upward longwave radiation ($R_l\uparrow$) can be expressed as

$$R_l\uparrow = \sigma\varepsilon_s T_s^4 + (1-\varepsilon_s)R_l\downarrow \tag{10}$$

where ε_s is the land surface emissivity and T_s is the LST (in Kelvin). MOD/MYD11 provides the daily LST values retrieved by using the generalized split-window algorithm (Wan and Dozier, 1996) and emissivities in bands 31 and 32 estimated using the classification-based emissivity method (Snyder and Wan, 1998). The ε_s value was calculated by using the following nonlinear formula (Liang, 2004):

$$\varepsilon_s = 0.273 + 1.778\varepsilon_{31} - 1.807\varepsilon_{31}\varepsilon_{32} - 1.037\varepsilon_{32} + 1.774\varepsilon_{32}^2 \tag{11}$$

where ε_{31} and ε_{32} denote the emissivities in bands 31 and 32, respectively.

2.2.5. *Quantitative measures to evaluate MODIS-derived variables*

To evaluate the performances of the MODIS-derived variables, the mean error (ME), root-mean-square error (RMSE), normalized RMSE (NRMSE), systematic RMSE ($RMSE_s$), unsystematic RMSE ($RMSE_u$), proportion of $RMSE_s$ ($PRMSE_s$) to RMSE, and proportion of $RMSE_u$ ($PRMSE_u$) to RMSE were computed.

$$ME = \frac{1}{n}\sum_{i=1}^{n} x_s - x_o \tag{12}$$

$$RMSE = \left[\frac{1}{n}\sum_{i=1}^{n}(x_s - x_o)^2\right]^{1/2}; \quad NRMSE = \frac{[(1/n)\sum_{i=1}^{n}(x_s - x_o)^2]^{1/2}}{(1/n)\sum_{i=1}^{n} x_o} \tag{13}$$

$$RMSE_s = \left[\frac{1}{n}\sum_{i=1}^{n}(\hat{x}_s - x_o)^2\right]^{1/2}; \quad RMSE_u = \left[\frac{1}{n}\sum_{i=1}^{n}(x_s - \hat{x}_s)^2\right]^{1/2} \tag{14}$$

$$PRMSE_s = \frac{(RMSE_s)^2}{(RMSE)^2}; \qquad PRMSE_u = \frac{(RMSE_u)^2}{(RMSE)^2} \tag{15}$$

where x_s and x_o are the simulated and measured values, respectively, i is the ith sample, n is the number of images over the study duration and $\hat{x}_s$ is the value of the linear regression of x_s on x_o (i.e., $\hat{x}_s = a_1 + a_2 x_o$, where a_1 and a_2 denote the intercept and slope, respectively).

ME is a measure of the bias for model performance. RMSE indicates the overall measure of the model accuracy. For comparing the RMSE values between the different sites, NRMSE – a relative measure of the RMSE – is used. For verifying whether the RMSE is induced by systematic or unsystematic errors, RMSE is divided into two components (namely, $RMSE_2 = RMSE_s^2 + RMSE_u^2$) (Anderson et al., 1997; Willmott, 1982). Each contribution to the RMSE is quantified using $PRMSE_s$ and $PRMSE_u$, which measures the proportion of the total RMSE arising from systematic and unsystematic biases, respectively.

2.2.6. *Uncertainty analysis*

To evaluate the error propagation in the calculation of R_n, we used the method of moments (Talyor, 1997):

$$s_{\bar{R}_n} = \sqrt{\sum_{j=1}^{4}\left(\frac{\partial R_n}{\partial x_j}s_{\bar{x}_j}\right)^2 + 2\sum_{j=1}^{4}\sum_{k=j+1}^{4} r_{x_j x_k}\left(\frac{\partial R_n}{\partial x_j}s_{\bar{x}_j}\right)\left(\frac{\partial R_n}{\partial x_k}s_{\bar{x}_k}\right)} \tag{16}$$

where s is the standard error, x_j and x_k are the four radiation components, and $r_{x_j x_k}$ is the correlation coefficient between x_j and x_k. This method is a general technique for estimating the moments of the variables under consideration. Here, we use the first-order second moment uncertainty analysis because R_n is a simple algebraic sum of four radiation components (Eq. (1)). We examined the sensitivity of $s_{\bar{R}_n}$ up to a tenfold change in the standard errors of the four individual components.

2.3. *Semivariogram analysis*

A semivariogram analysis was used to investigate the effect of land surface heterogeneity on the albedo and LST of 1 km^2

MODIS products. This method has been widely used to quantify the scales of land surface heterogeneity (Cohen et al., 1990; Curran, 1988; Kim et al., 2006a). We used high-resolution satellite images (visual and near-infrared band: 30 m; thermal band: 60 m) of Landsat ETM+ selected from a growing season (September 23, 2001) and a dormant season (14 February 2002) after geometric correction using a digital map (1:5000) and atmospheric correction using the COST model (Chavez, 1996). The LST was calculated from the digital number of the thermal band using conversion equations (http://ltpwww.gsfc.nasa.gov/IAS/handbook/). Broadband albedos were calculated by using a linear formula using three bands (Liang, 2004):

$$\alpha = 0.526\alpha_2 + 0.3139\alpha_4 + 0.112\alpha_7 \quad (17)$$

where α_2, α_4, and α_7 are the reflectances of ETM+ bands 2 (0.52–0.60 μm), 4 (0.72–0.90 μm), and 7 (2.09–2.35 μm), respectively.

Semivariance (γ^*) is a measure to estimate the variability in the data at a certain (space or time) interval and can be estimated as (Davis, 1986)

$$\gamma^*(h) = \frac{1}{2N(h)}\sum_{i=1}^{N(h)}[z(x_i) - z(x_i + h)]^2, \quad (18)$$

where $N(h)$ is the number of experimental pairs ($z(x_i)$ and $z(x_i + h)$) of data separated by the vector h. A semivariogram is a plot of γ^* at each separation (or lag) distance (h), where the *sill* of the semivariogram is defined as the value of γ^* that no longer increases and the *range* of the semivariogram is the value of h that corresponds to the *sill*, respectively. The *range* indicates the neighborhood within which all the locations are interrelated.

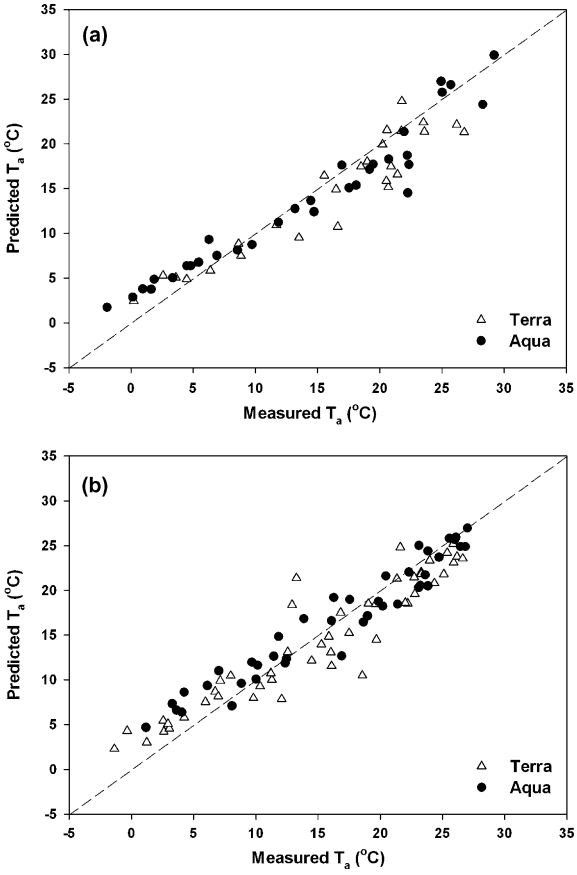

Fig. 3 – Comparison of measured and MODIS derived air temperature (T_a) over (a) the DK site and (b) the FK site. Dash line indicates 1:1 line.

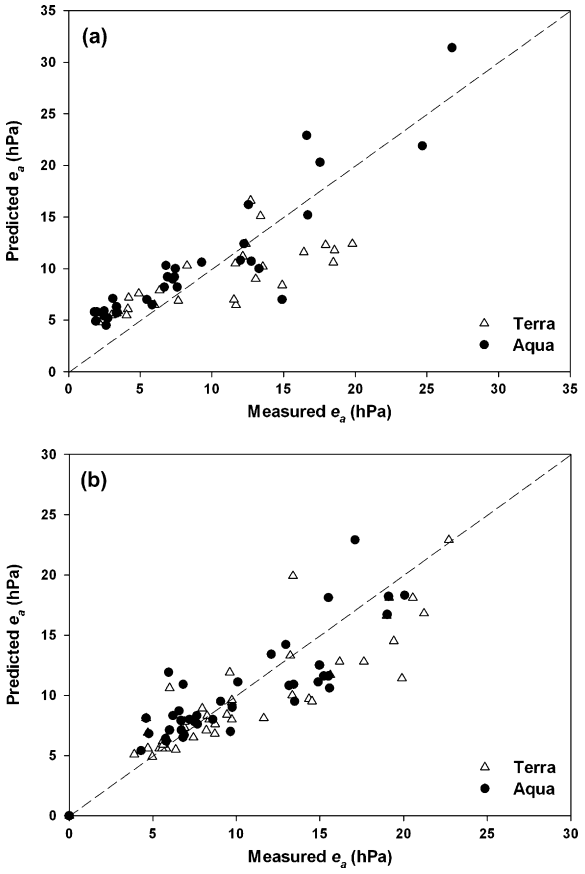

Fig. 4 – Comparison of measured and MODIS derived actual vapor pressure (e_a) over (a) the DK site and (b) the FK site. Dash line indicates 1:1 line.

3. Results

3.1. Input variables

The MODIS-derived air temperature values showed good agreement with the flux tower measurements at the DK site with the RMSE values of 2.9 and 2.6 °C for the Terra and Aqua MODIS systems, respectively, and the NRMSE values of 0.19 for both the systems. For the FK site, the corresponding errors were quite similar (Fig. 3). The magnitudes of these errors were generally smaller than those reported in previous studies in which the relationship of the surface temperature and vegetation index were used from AVHRR (5.4 °C over western Oregon, USA (Goward et al., 1994); 4.2 °C over boreal forests (Czajkowski et al., 1997); 2.9 °C over northeastern Kansas (Prihodko and Goward, 1997); 3.5, 1.7, 2.2, and 4.9 °C for FIFE, HAPEX, BOREAS, and Red-Arkansas basin, respectively (Prince et al., 1998)) and by using Terra MODIS (2.5 °C over an

agricultural area in Denmark (Houborg and Soegaard, 2004) and 5.0 °C over the Southern Great Plains, USA (Bisht et al., 2005)).

The actual vapor pressure (e_a) showed a reasonable agreement with the field measurements at the DK site with RMSE values of 4.0 and 3.2 hPa and NRMSE values of 0.39 and 0.36 for the Terra and Aqua MODIS systems, respectively. The corresponding errors were much smaller at the FK site (Fig. 4). The RMSE values at both these sites were greater than those estimated from Terra (~1.4 hPa), as reported by Houborg and Soegaard (2004).

The albedos measured during the Terra overpass were averaged over 16 days in accordance with the MODIS albedo product. The obtained albedo showed a good agreement with the field measurements at the DK site (RMSE = 0.03, NRMSE = 0.25, and coefficient of determination $r^2 = 0.32$; Fig. 5). For the FK site, the RMSE and NRMSE values were 0.03 and 0.17, respectively, but the r^2 value was as low as 0.03 and the ME value was −0.02 (Table 2). The error magnitudes at the FK site were comparable to those reported for the paddy fields in Japan (RMSE = 0.026 and NRMSE = 0.15) (Susaki et al., 2007).

3.2. *Four components of net radiation*

All the statistical information about the four radiation components is summarized in Table 3. We can see that $R_s\downarrow$ was consistently overestimated at the DK site with ME values of 32 and 57 W m^{-2} for Terra and Aqua, respectively. For the FK site, it was slightly overestimated for Terra (ME = 13 W m^{-2}), but there was virtually no bias for Aqua (ME = 0.3 W m^{-2}). Overall, the retrieved $R_s\downarrow$ values agreed well with the field measurements at the DK site: the RMSE values were 41 and 65 W m^{-2} and the NRMSE values were 0.06 and 0.10 for the Terra and Aqua MODIS systems, respectively. For the FK site, the agreement was much better (Fig. 6a and e). Our results reveal smaller RMSE values than those reported in other studies that have used GOES (~135 W m^{-2}; Jacobs et al., 2002), but they are comparable to the studies that have employed the Terra MODIS data (~50 W m^{-2}; Houborg and Soegaard, 2004; Bisht et al., 2005). Further, we attempted to estimate $R_s\downarrow$ according to Bisht et al. (2005) based on the Zillmann (1972), which yielded much larger RMSE values of 124 and 118 W m^{-2} at the DK site and 100 and 95 W m^{-2} at the FK site for Terra and Aqua, respectively.

$R_s\uparrow$ was slightly overestimated at the DK site (with ME values of 3 and 13 W m^{-2} for Terra and Aqua), but it was underestimated at the FK site (−21 and −29 W m^{-2} for Terra and Aqua) (Fig. 6b and f). Overall, the DK site showed a better agreement with the field measurements with RMSE values of ~10 W m^{-2} and higher r^2 values. For both DK and FK sites, the RMSE values of Aqua were mainly induced by systematic errors (with $PRMSE_s$ values of 0.92 and 0.77, respectively).

$R_l\downarrow$ showed a good agreement with the field measurements; RMSE values of ~20 W m^{-2} were obtained at both the sites (Fig. 6c and g). These errors are comparable to the two Denmark sites (39 and 30 W m^{-2}), which used the same model (Kjaersgaard et al., 2007). When using the globally optimized value of m (46.5) (Eq. (8)), we found that there were consistent positive biases (ME values of 23 and 29 W m^{-2} for Terra and Aqua) at the FK site, whereas negative biases (ME values of −30 and −11 W m^{-2} for Terra and Aqua) at the DK site (Table 4). This issue has been discussed in the next section.

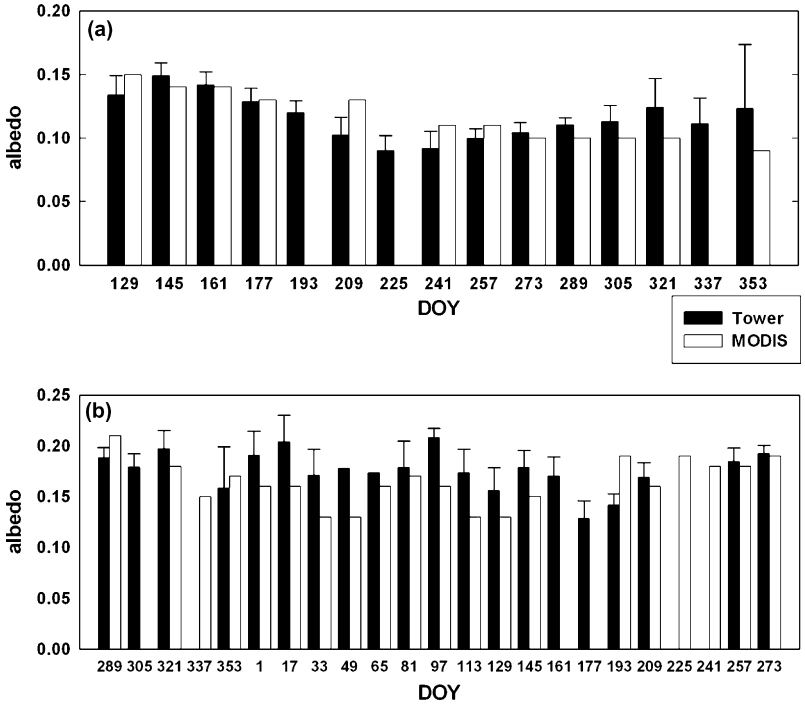

Fig. 5 – Comparison of measured and MODIS derived albedo over (a) the DK site and (b) the FK site. Measured albedos at Terra overpass time were averaged over 16-day in accordance with MODIS albedo product. Error bar means standard deviation for 16-day.

Table 2 – Stastistics for air temperature (T_a, °C,), actual vapor pressure (e_a, hPa), and albedo

Site	Variables	Platforms	N	a	b	r^2	$\bar{x}_o$	ME	RMSE	NRMSE
DK	T_a	Terra	27	1.8	0.80	0.40	15.5	−1.2	2.9	0.19
		Aqua	32	2.3	0.82	0.93	13.7	−0.2	2.6	0.19
	e_a	Terra	27	4.8	0.42	0.55	10.3	−1.2	4.0	0.39
		Aqua	32	2.9	0.85	0.82	8.8	1.5	3.2	0.36
	Albedo	Terra	12	0.04	0.64	0.32	0.12	0	0.03	0.25
FK	T_a	Terra	45	2.6	0.78	0.91	14.8	−0.58	2.9	0.20
		Aqua	42	3.5	0.80	0.94	16.6	0.24	2.3	0.14
	e_a	Terra	46	2.45	0.68	0.74	10.7	−0.93	2.9	0.27
		Aqua	38	2.84	0.73	0.70	10.3	0.07	2.5	0.24
	Albedo	Terra	17	0.12	0.24	0.03	0.18	−0.02	0.03	0.17

N: number of samples, a: intercept, b: slope, $\bar{x}_o$: measured mean, ME: mean error, RMSE: root mean square error, NRMSE: normalized RMSE.

$R_l\uparrow$ was underestimated at both the sites with ME values of −19 and −18 W m^{-2} for Terra and Aqua at the DK site and −11 and −6 W m^{-2} at the FK site, respectively (Fig. 6d and h). Overall, the agreement with the field measurements was very good with RMSE values of 20 and ~10 W m^{-2} at the DK and FK sites, respectively. It is noteworthy that the RMSE value at the DK site was induced mainly by systematic errors ($PRMSE_s$ values of 0.85 and 0.95 for Terra and Aqua, respectively) and by unsystematic errors ($PRMSE_u$ values of 0.63 and 0.69 for Terra and Aqua, respectively) at the FK site.

3.3. Net radiation

R_n was successfully reproduced at both the sites for both Terra and Aqua with relatively small errors (Fig. 7 and Table 3). The RMSE values ranged from 33 to 61 W m^{-2}, which are less than the values obtained in other studies that have employed the MODIS Terra data (~74 W m^{-2}; Bisht et al., 2005) and GOES (~108 W m^{-2}; Jacobs et al., 2002). The ME value was positive for both the sites for both Terra and Aqua (Table 3). All the cases showed a positive ME value mainly due to the overestimation

Table 3 – Stastistics for shortwave downward and upward radiation ($R_s\downarrow$, $R_s\uparrow$) and longwave downward and upward radiation ($R_l\uparrow$, $R_l\downarrow$), and net radiation (R_{net}) for the DK and FK sites

Site	Variables	Platforms	r^2	$\bar{x}_o$	ME	RMSE	$PRMSE_s$	$PRMSE_u$	NRMSE
DK	$R_s\downarrow$	Terra	0.98	689	32	41	0.71	0.29	0.06
		Aqua	0.94	598	57	65	0.83	0.17	0.10
	$R_s\uparrow$	Terra	0.98	83	3	5	0.19	0.81	0.06
		Aqua	0.91	50	13	14	0.92	0.08	0.27
	$R_l\downarrow$	Terra	0.90	307	−15	24	0.75	0.25	0.08
		Aqua	0.91	309	3	18	0.46	0.54	0.06
	$R_l\uparrow$	Terra	0.96	417	−19	21	0.85	0.15	0.05
		Aqua	0.98	405	−18	20	0.95	0.05	0.05
	R_{net}	Terra	0.97	551	33	46	0.77	0.23	0.08
		Aqua	0.97	486	61	65	0.92	0.08	0.13
FK	$R_s\downarrow$	Terra	0.98	726	13	24	0.34	0.66	0.03
		Aqua	0.97	787	0.3	19	0.11	0.89	0.03
	$R_s\uparrow$	Terra	0.49	136	−21	28	0.55	0.45	0.24
		Aqua	0.32	147	−29	35	0.77	0.23	0.30
	$R_l\downarrow$	Terra	0.88	274	−3	20	0.49	0.51	0.07
		Aqua	0.87	281	3	15	0.48	0.52	0.05
	$R_l\uparrow$	Terra	0.95	418	−11	15	0.37	0.63	0.04
		Aqua	0.94	425	−6	12	0.31	0.69	0.03
	R_{net}	Terra	0.96	506	41	51	0.82	0.18	0.10
		Aqua	0.92	517	38	47	0.73	0.27	0.09

Sample numbers of Terra and Aqua for the DK site are 17 and 26. Sample numbers of Terra and Aqua for the FK site are 41 and 30. The unit of radiations is W m^{-2}. The unit of $\bar{x}_o$, ME and RMSE is W m^{-2}. $PRMSE_s$, $PRMSE_u$, and NRMSE are unitless. $\bar{x}_o$ is the measured mean, ME is the mean error, RMSE is the root mean square error, $PRMSE_s$ is the proportion of $RMSE_s$ to RMSE, $PRMSE_u$ is the proportion of $RMSE_u$ to RMSE, and NRMSE is the normalized RMSE.

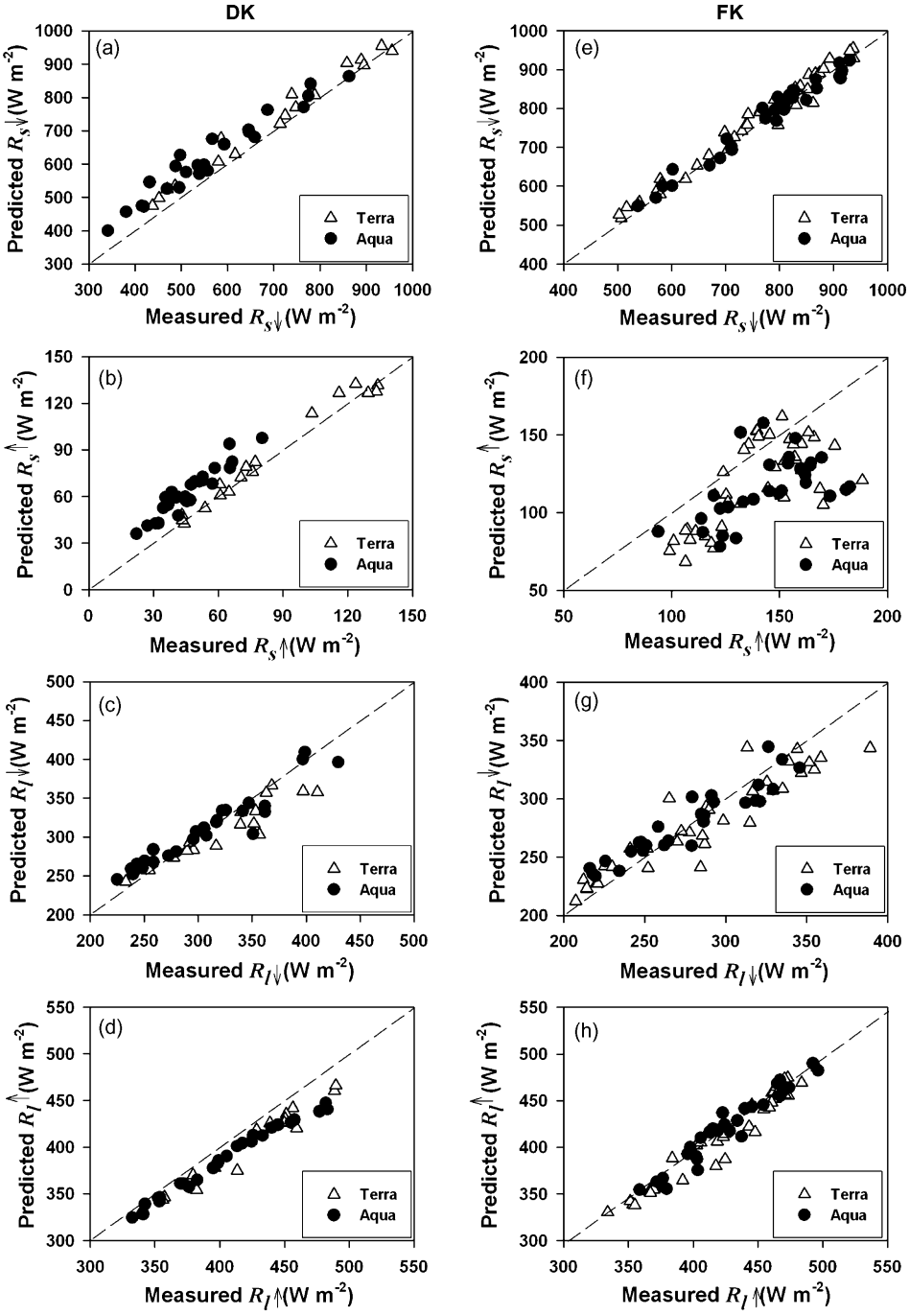

Fig. 6 – Comparison of measured and MODIS derived four radiation components over the DK and FK sited. R_s and R_l are the shortwave and longwave radiation, respectively. ↑ and ↓ are the upwelling and downwelling streams, respectively. Dash line indicates 1:1 line.

of $R_s\downarrow$ with an underestimation of $R_l\uparrow$ at the DK site and underestimation of $R_s\uparrow$ at the FK site. Further, we examined how the standard error of R_n responded to changes (from two- to tenfold increase) in each standard error of the four radiation components. As expected, the uncertainty in the retrieval of R_n was mainly dependent on the accuracy of $R_l\downarrow$ followed by $R_l\downarrow$, $R_l\uparrow$, and $R_s\uparrow$ (in this particular order) at the DK and FK sites.

Diurnal changes in the MODIS-derived R_n values (i.e., R_n at the Aqua overpass time minus R_n at the Terra overpass time on the same day) were tested against the field data on the days when both Terra- and Aqua-derived R_n values were successfully retrieved (Fig. 8). The DK site showed a better agreement ($n = 6$, $r^2 = 0.37$, RMSE = 29 W m^{-2}) than the FK site ($n = 14$, $r^2 = 0.46$, and RMSE = 59 W m^{-2}). The difference in the ME values between Terra and Aqua was greater at the FK site (31 W m^{-2}) than at the DK site (6 W m^{-2}) (Table 3), causing a larger discrepancy in the diurnal changes in R_n at the FK site. The measured diurnal changes in R_n were averaged to be

Table 4 – Stastistics for errors of downward longwave radiation ($R_l\downarrow$) arising from coefficient m (Eq. (8)) and input data (air temperature and actual vapor pressure) at the DK and FK sites

Site	Input data	Terra $R_l\downarrow$		Aqua $R_l\downarrow$	
		ME (W m^{-2})	RMSE (W m^{-2})	ME (W m^{-2})	RMSE (W m^{-2})
DK	Field data with m = 46.5	−15	17	−13	14
	Field data with m = 69.7	−1	9	−1	6
	[a]MODIS data with m = 69.7	−15	24	3	18
	MODIS data with m = 46.5	−30	37	−11	23
FK	Field data with m = 46.5	27	28	27	29
	Field data with m = 14.8	2	13	1	11
	[a]MODIS data with m = 14.8	−3	20	3	15
	MODIS data with m = 46.5	23	29	29	33

The original value of m is 46.5, globally optimized value (Prata, 1996). The calibrated m is 69.7 and 14.8 for DK and FK sites, respectively.
[a] In this study, $R_l\downarrow$ was calculated from this method.

−20 W m^{-2} at the DK site and 37 W m^{-2} at the FK site, which were smaller than the MODIS-derived RMSE values (29 W m^{-2} at the DK site and 59 W m^{-2} at the FK site). It indicates that MODIS-derived R_n is inappropriate to represent the diurnal changes in R_n.

3.4. *Acquisition rate*

We tested the acquisition rate (i.e., the number of MODIS-derived R_n values over the number of flux tower measurements at the same time of the Terra and Aqua overpasses) of the MODIS-derived R_n at the FK site (Fig. 9). Although the perfectly clear pixels (i.e., 25 pixels within a 5 km × 5 km pixel) were used in this study to ensure clarity, half-clear pixels also showed comparable RMSE values with almost double the acquisition rate for both Terra and Aqua. This indicates that the acquisition rate can be increased depending on the RMSE level. However, the overall acquisition rate at the half-clear pixels was less than 25% because of frequent cloud covers, long monsoon seasons, and difficulties in obtaining good-quality input variables from MODIS.

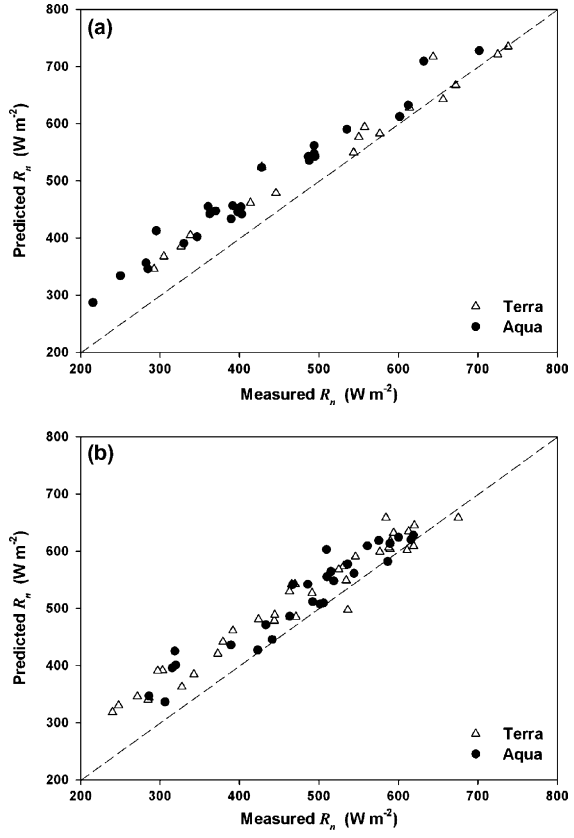

Fig. 7 – Comparison of measured and MODIS derived net radiation (R_n) over (a) the DK site and (b) the FK site. Dash line indicates 1:1 line.

4. Discussion

Spatial heterogeneity and complex topography are the characteristics of Korean landscapes. The DK site is a *Quercus*-dominated forest with understory vegetation present in complex terrain, while the FK site is composed of heterogeneous patch mosaics on a relatively flat terrain (Fig. 3). Such landscape characteristics could result in different source in error in R_n estimated at the two sites.

The effect of topography on $R_s\downarrow$ in complex terrain has been well recognized and modeled by many researchers (Dubayah, 1992, 1994; Dubayah and Loechel, 1997; Dubayah and Rich, 1995; Flint and Childs, 1987; Kang et al., 2002; Wang et al., 2005). Our $R_s\downarrow$ scheme considers both direct and diffuse components for flat terrain, but it does not consider irradiance obstructed by adjacent topography and reflected from nearby terrain. The adjacent topography affects the direct and diffuse components of $R_s\downarrow$ by determining the horizon angles of sunrise and sunset and by reshaping the sky openness (i.e., the sky-view factor defined as the unobstructed portion of the sky at any given point (Dozier and Frew, 1990)). At the DK site, the obstruction of direct radiation by the adjacent topography (i.e., shading) does not matter because the solar altitude is always greater than the local horizon angle at the MOD/MYD overpass time. However, the diffuse radiation is partially obstructed by the adjacent topography during the entire daytime, thereby resulting in lower diffuse radiation than that for the flat horizon. Kang et al. (2002) reported a sky-view factor ranging from 0.82 to 0.94 at a mountain area near the DK site. Hence, the $R_s\downarrow$ value measured in a catchment valley at the DK site can induce systematic overestimations in the comparison of $R_s\downarrow$

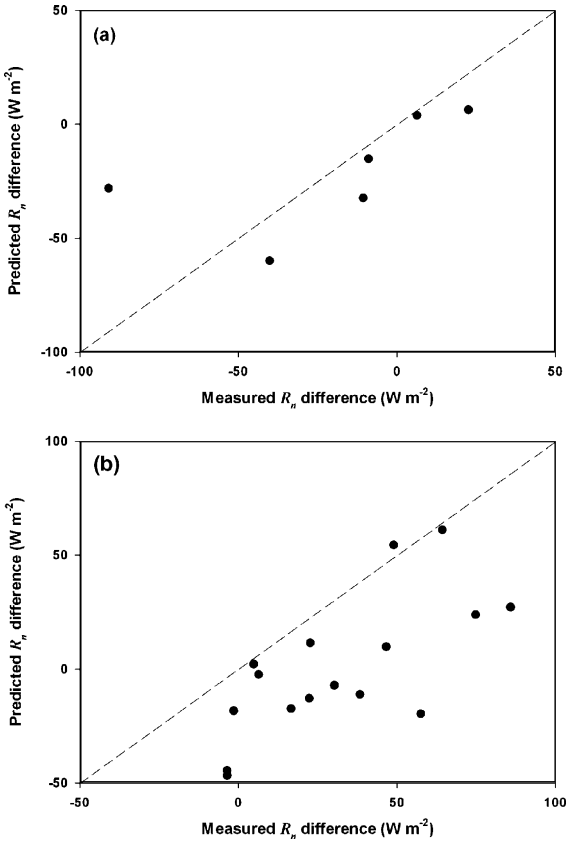

Fig. 8 – Comparison of measured and MODIS derived net radiation difference (Aqua overpass time minus Terra overpass time) over (a) the DK site and (b) the FK site. Dash line indicates 1:1 line.

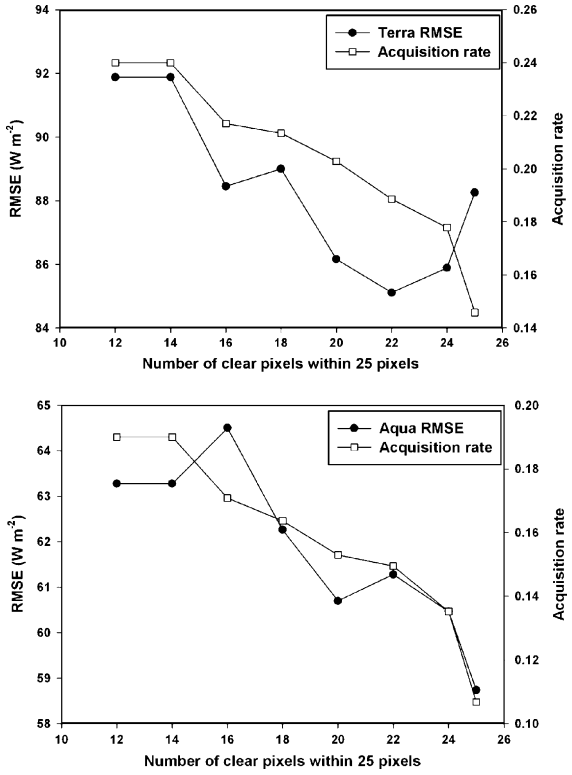

Fig. 9 – The changes of RMSE and acquisition rate of net radiation with the number of clear pixels within 25 pixels for (a) Terra and (b) Aqua over the FK site. MOD/MYD07 product (5 km × 5 km) provides the number of clear pixels (1 km × 1 km) within each pixel (5 km × 5 km). The 100% acquisition rate was assumed as the number of tower measurement. The numbers of tower measurement during the analysis period for the FK site were 281 and 280 days for Terra and Aqua, respectively.

estimated from the flat-terrain-based MODIS data. In fact, the ME values at the DK site were positive for both Terra and Aqua and the RMSE values for both Terra and Aqua were dominated by systematic errors, as shown in Table 3. Such a systematic overestimation of $R_s\downarrow$ at the DK site suggests that the terrain complexity should be taken into account when using coarse remote sensing data such as MODIS and AVHRR. We found that the scheme by Bird and Hulstrom (1981) performed excellently for the flat-terrain FK site (Fig. 6e).

The modeling of $R_l\downarrow$ is a challenge because of the presence of complex atmospheric constituents even under clear sky conditions, which affect the atmospheric emissivity in a variety of ways. In this study, the MODIS-derived $R_l\downarrow$ showed a good agreement with the field measurements. However, it should be noted that the coefficient m was calibrated at each site. The error sources arising from the input data and model parameterization scheme are listed in Table 4. When using the original value of m (46.5) with the measured input data, the ME values at the DK and FK sites were approximately −14 and 27 W m^{-2}, respectively, indicating that the parameterization scheme itself induced consistent biases. When using the locally fitted m values with the measured input data, the errors were substantially reduced. The MODIS-derived $R_l\downarrow$ values along with the locally fitted m values show comparable errors with that in previous case at the FK site, indicating that the error sources from the MODIS-derived input data are insignificant. For the DK site, the errors of the MODIS-derived input data significantly increased the errors of $R_l\downarrow$. For both the sites, when using the globally optimized value (46.5) with the MODIS-derived input variables, the errors were substantially amplified by the combined errors from the parameterization scheme and MODIS uncertainties. We found that other $R_l\downarrow$ models (Brutsaert, 1975; Idso, 1981; Satterlund, 1979; Swinbank, 1963) also showed similar biases or even larger errors at both the sites, suggesting a necessity to revise and refine the $R_l\downarrow$ scheme (particularly the emissivity scheme) applicable for various atmospheric conditions.

Both $R_s\uparrow$ and $R_l\uparrow$ are influenced by land cover heterogeneity (Jin et al., 2003; Salomon et al., 2006). At the FK site, $R_s\uparrow$ was significantly underestimated for both Terra and Aqua. It is mainly due to the underestimation of the MODIS albedo (Fig. 5), partly caused by land surface heterogeneity. The ground-based measurement of the albedo at the FK site did not show a clear seasonal change, probably reflecting the complex land use patterns (i.e., scattered rice paddies with seasonally cultivated crops). Contrary to previous studies (Jin et al., 2003; Salomon et al., 2006), we observed large ME and RMSE values

for the albedo during the growing season, indicating the necessity of considering land cover heterogeneity even during the growing season.

The large discrepancy of $R_s\uparrow$ at the FK site and a better agreement at the DK site can be explained partly by examining the scale of the spatial and temporal heterogeneities. Spatial heterogeneity involves at least three different scales: (1) footprint of the ground-based radiation measurement, (2) heterogeneity of the land cover/use associated with the parameters of interest (e.g., albedo, LST, and so on), and (3) MODIS pixel/product. First, the radiation footprint can be defined by the sensor height and the radius of the source area (e.g., Schmid, 1997). The radiometers were installed ~20 m above the forest canopy at the DK site and ~10 m above the canopy at the FK site. Hence, ~90% of the source area for the upwelling radiation measurements was within a radius of 60 m at the DK site and 30 m at the FK site, which is considerably smaller than the MODIS pixel (i.e., 1 km^2). Second, the semivariogram analysis indicated that the spatial structures of the broadband albedo at the FK site had a *range* of ~300 m during both the growing and dormant seasons. Here, patch mosaics with similar albedos are scattered within the image domain, inducing spatial heterogeneity in the albedo. At the DK site, on the other hand, both the *sill* and *range* of the albedo were not associated with the larger patches of the hillslope aspects. In other words, the DK site was more homogeneous than the FK site in terms of albedo, since the former had patches larger than the MODIS pixel whereas the latter had smaller patches at a scale of approximately 300 m. Next, the large discrepancy at the FK site can be attributed to temporal heterogeneity. The FK site is composed of various cultivated crop patches with bare soils. When considering the irregularity of cultivation activity, rainfall and snowfall, the 16-day composite of the MODIS albedo product could not conform to the instantaneous estimation of $R_s\uparrow$. This fact has been supported by the irregular standard deviations in the ground-based albedos at the MODIS overpass time over 16 days (Fig. 5b).

It is noteworthy that $R_s\uparrow$ for Aqua at the DK site showed systematic overestimation (ME = 13 W m^{-2}). The measured albedo showed diurnal variations during the study period at the DK site from 0.11 (between 10:30 and 11:30 a.m.) to 0.09 (between 1:30 and 2:30 p.m.). Further, it should be noted that we applied the MOD43B3 albedo product (from Terra) to the $R_s\uparrow$ estimation for both Terra and Aqua, causing an overestimation of $R_s\uparrow$ for Aqua. For both the sites, the RMSE value of Aqua $R_s\uparrow$ was dominated by systematic errors ($PRMSE_s$ = 0.90, see Table 3), suggesting that it is necessary to use independent albedo values for Terra and Aqua to minimize the errors.

Surprisingly, our results at the heterogeneous FK site showed very good agreement between $R_l\uparrow$ and the field measurements, contrary to those for $R_s\uparrow$ (Fig. 6f and h). Interestingly, geostatistical analyses of the LST images during the growing season at the FK site showed a range of ~600 m, which corresponds to the size of the residential areas at the site. During the winter season at the FK site, both the *sill* and *range* of the LST did not exist within 1 km^2, indicating the existence of large patches greater than 1 km. At the DK site, the LST images had no *sill* and *range* within 1 km^2 during both the growing and dormant seasons. The large patches are related to the aspect of the hillslopes at the DK site and bare soil (no crops in the agricultural fields) at the FK site. In terms of the LST (a major determinant of $R_l\uparrow$), both the sites had larger scales of spatial heterogeneity (>0.6–1 km), resulting in better agreement between the modeled and measured $R_l\uparrow$.

Further, it should be noted that the RMSE value at the FK site was dominated by unsystematic errors ($PRMSE_u$ values of 0.61 and 0.71 for Terra and Aqua, respectively), possibly induced by complex diurnal and seasonal LST variations in the heterogeneous land cover within the tower footprint and the MODIS LST extent (1 km). At the DK site, both Terra and Aqua may have underestimated $R_l\uparrow$ due to the terrain effect, which alters the LST because of the terrain angular effect and adjacent terrain emittance effect. Liu et al. (2006) reported that the LST increased by 0.4 K after correcting the combined effects.

5. Summary and conclusions

In this study, we employed a scheme for retrieving the four radiation components and R_n from various MODIS land and atmosphere products over a deciduous forest in a complex terrain (DK) and a farmland with heterogeneous patch mosaics (FK) in Korea. The main results of this study can be summarized as follows:

(1) MODIS-derived air temperature and vapor pressure values were successfully retrieved with a reasonable accuracy for both the Terra and Aqua satellites.
(2) The MODIS albedo derived from Terra (MOD43B3) showed a good agreement with the field measurement at the DK site, but it was significantly underestimated at the FK site due to land surface heterogeneity and mismatch between the instantaneous tower-measured albedo and 16-day composite MODIS albedo. The application of MOD43B3 for the afternoon (Aqua) induced significant systematic errors at both the sites due to diurnally varying albedo. It is necessary to develop both Terra- and Aqua-derived albedos for an accurate retrieval of the diurnal variation in R_n.
(3) For $R_s\downarrow$, the DK site showed an overestimation with higher NRMSE values for both Terra and Aqua than those at the FK site, implying that the topographic effect should be considered at the DK site.
(4) $R_l\downarrow$ was successfully retrieved with good accuracy. However, the emissivity scheme should be further revised and refined such that it can be applied to various atmospheric conditions.
(5) $R_l\uparrow$ was systematically underestimated at the DK site, implying that the terrain angular effect and adjacent terrain emittance effect may reduce the LST (Liu et al., 2006). The RMSE value of $R_l\uparrow$ at the FK site was mainly controlled by unsystematic errors, possibly induced by land surface heterogeneity.
(6) The standard error of R_n was mainly dependent on that of $R_s\downarrow$ at both the sites. R_n was successfully retrieved, but both these sites exhibited positive ME. It was mainly due to the overestimation of $R_s\downarrow$ with the underestimation of $R_l\uparrow$ at the DK site and the underestimation of $R_s\uparrow$ at the FK site. It

implies that the errors of the four radiation components should be thoroughly tested.

(7) The retrieval of the diurnal variation in R_n was questionable because the ME value of Terra was greater than that of Aqua.

Our results suggest that the MODIS sensors onboard the Terra and Aqua platforms provide a great opportunity for better understanding the land surface energy balance across different landscapes. However, when applying the MODIS-derived land surface radiation components over complex and heterogeneous landscapes, the scale mismatch among the radiometer footprint, heterogeneity of the land surface properties, and MODIS extent should be considered in both the algorithm development and validation processes.

Acknowledgements

We heartily appreciate Drs. Rasmus Houborg (U Copenhagen) and Maosheng Zhao (U Montana) for providing IDL code and helping MODIS processing, and Dr. Jinkyu Hong for providing constructive comments. This work was supported by the Sustainable Water Resources Research Center of the 21st Century Frontier Program (Grant code: 1-8-2); Eco-Technopia 21 Project of the Ministry of Environment; the Basic Research Project of the Korea Institute of Geoscience and Mineral Resources (KIGAM); and BK21 Program of the Ministry of Education and Human Resource Management of Korea.

REFERENCES

Anderson, M.C., Norman, J.M., Diak, G.R., Kustas, W.P., Mecikalski, J.R., 1997. A two-source time-integrated model for estimating surface fluxes using thermal infrared remote sensing. Remote Sens. Environ. 60 (2), 195–216.

Annear, R.L., Wells, S.A., 2007. A comparison of five models for estimating clear-sky solar radiation. Water Resour. Res. 43 (W10415), doi:10.1029/2006WR005055.

Baldocchi, D.D., Krebs, T., Leclerc, M.Y., 2005. ''Wet/dry Daisyworld'': a conceptual tool for quantifying the spatial scaling of heterogeneous landscapes and its impact on the subgrid variability of energy fluxes. Tellus 57B, 175–188.

Bird, R.E., Hulstrom, R.L., 1981. A simplified clear sky model for direct and diffuse insolation on horizontal surfaces. SERI Report TR-642-761. Golden, USA.

Bisht, G., Venturini, V., Islam, S., Jiang, L., 2005. Estimation of the net radiation using MODIS (moderate resolution imaging spectroradiometer) data for clear sky days. Remote Sens. Environ. 97 (1), 52–67.

Boegh, E., Soegaard, H., Thomsen, A., 2002. Evaluating evapotranspiration rates and surface conditions using Landsat TM to estimate atmospheric resistance and surface resistance. Remote Sens. Environ. 79, 329–343.

Brunsell, N.A., Gillies, R.R., 2003. Scale issues in land–atmosphere interactions: implications for remote sensing of the surface energy balance. Agric. Forest Meteorol. 117, 203–221.

Brutsaert, W., 1975. Derivable formula for long-wave radiation from clear skies. Water Resour. Res. 11 (5), 742–744.

Chavez Jr., P.S., 1996. Image-based atmospheric corrections: revisited and improved. Photogrammetric Eng. Remote Sens. 62 (9), 1025–1036.

Choi, T., Lim, J.H., Chun, J.H., Lee, D., Kim, J., 2005. Microclimatological characteristics observed from the flux tower in Gwangneung forest watershed. Kor. J. Agric. Forest Meteorol. 7 (1), 35–44.

Cohen, W.B., Spies, T.A., Bradshaw, G.A., 1990. Semivariograms of digital imagery for analysis of conifer canopy structure. Remote Sens. Environ. 34, 167–178.

Curran, P.J., 1988. The semivariograms in remote sensing: an introduction. Remote Sens. Environ. 24, 493–507.

Czajkowski, K.P., Mulhern, T., Goward, S.N., Cihlar, J., Dubayah, R.O., Prince, S.D., 1997. Biospheric environmental monitoring at BOREAS with AVHRR observations. J. Geophys. Res. 102 (D24), 29651–29662.

Davis, J., 1986. Statistics and Data Analysis in Geology. John Wiley & Sons, 637 pp.

Diak, G.R., Mecikalski, J.R., Anderson, M.C., Norman, J.M., Kustas, W.P., Torn, R.D., DeWolf, R.L., 2004. Estimating land surface energy budgets from space: review and current efforts at the University of Wisconsin–Madison and USDA–ARS. Bull. Am. Meteorol. Soc. 85 (1), 65–78.

Dozier, J., Frew, J., 1990. Rapid calculation of terrain parameters for radiation modeling from digital elevation data. IEEE Trans. Geosci. Remote Sens. 28, 963–969.

Dubayah, R.C., 1992. Estimating net solar radiation using Landsat Thematic Mapper and digital elevation data. Water Resour. Res. 28 (9), 2469–2484.

Dubayah, R.C., 1994. Modeling a solar-radiation topoclimatology for the Rio-Grande river basin. J. Veg. Sci. 5 (5), 627–640.

Dubayah, R.C., Loechel, S., 1997. Modeling topographic solar radiation using GOES data. J. Appl. Meteorol. 36 (2), 141–154.

Dubayah, R.C., Rich, P.M., 1995. Topographic solar-radiation models for GIS. Int. J. Geographical Inform. Syst. 9 (4), 405–419.

Flint, A.L., Childs, S.W., 1987. Calculation of solar radiation in mountainous terrain. Agric. Forest Meteorol. 40 (3), 233–249.

Gautier, C., Diak, G.R., Masse, S., 1980. A simple physical model to estimate incident solar radiation at the surface from GOES satellite data. J. Appl. Meteorol. 19, 1005–1012.

Goward, S.N., Waring, R.H., Dye, D.G., Yang, J., 1994. Ecological remote sensing at OTTER: satellite macroscale observations. Ecol. Appl. 4 (2), 322–343.

Gratton, D.J., Howarth, P.J., Marceau, D.J., 1993. Using Landsat-5 thematic mapper and digital elevation data to determine the net radiation field of a Mountain Glacier. Remote Sens. Environ. 43 (3), 315–331.

Harries, J.E., Russell, J.E., Hanafin, J.A., Brindley, H., Futyan, J., Rufus, J., Kellock, S., Matthews, G., Wrigley, R., Last, A., Mueller, J., Mossavati, R., Ashmall, J., Sawyer, E., Parker, D., Caldwell, M., Allan, P.M., Smith, A., Bates, M.J., Coan, B., Stewart, B.C., Lepine, D.R., Cornwall, L.A., Corney, D.R., Ricketts, M.J., Drummond, D., Smart, D., Cutler, R., Dewitte, S., Clerbaux, N., Gonzalez, L., Ipe, A., Bertrand, C., Joukoff, A., Crommelynck, D., Nelms, N., Llewellyn-Jones, D.T., Butcher, G., Smith, G.L., Szewczyk, Z.P., Mlynczak, P.E., Slingo, A., Allan, R.P., Ringer, M.A., 2005. The geostationary earth radiation budget project. Bull. Am. Meteorol. Soc. 86 (7), 945–960.

Houborg, R.M., Soegaard, H., 2004. Regional simulation of ecosystem CO_2 and water vapor exchange for agricultural land using NOAA AVHRR and Terra MODIS satellite data. Application to Zealand, Denmark. Remote Sens. Environ. 93, 150–167.

Houborg, R., Soegaard, H., Boegh, E., 2007. Combining vegetation index and model inversion methods for the extraction of key vegetation biophysical parameters using Terra and

Aqua MODIS reflectance data. Remote Sens. Environ. 106 (1), 39–58.
Idso, S.B., 1981. A set of equations for full spectrum and 8–14 μm and 10.5–12.5 μm thermal-radiation from cloudless skies. Water Resour. Res. 17 (2), 295–304.
Jacob, F., Petitcolin, F., Schmugge, T., Vermote, E., French, A., Ogawa, K., 2004. Comparison of land surface emissivity and radiometric temperature derived from MODIS and ASTER sensors. Remote Sens. Environ. 90 (2), 137–152.
Jacobs, J.M., Myers, D.A., Anderson, M.C., Diak, G.R., 2002. GOES surface insolation to estimate wetlands evapotranspiration. J. Hydrol. 266 (1–2), 53–65.
Jin, Y.F., Schaaf, C.B., Woodcock, C.E., Gao, F., Li, X.W., Strahler, A.H., Lucht, W., Liang, S.L., 2003. Consistency of MODIS surface bidirectional reflectance distribution function and albedo retrievals. 2. Validation. J. Geophys. Res. 108 (D5), 4159, doi:10.1029/2002JD002804.
Justice, C.O., Vermote, E., Townshend, J.R.G., Defries, R., Roy, D.P., Hall, D.K., Salomonson, V.V., Privette, J.L., Riggs, G., Strahler, A., Lucht, W., Myneni, R.B., Knyazikhin, Y., Running, S.W., Nemani, R.R., Wan, Z.M., Huete, A.R., van Leeuwen, W., Wolfe, R.E., Giglio, L., Muller, J.P., Lewis, P., Barnsley, M.J., 1998. The moderate resolution imaging spectroradiometer (MODIS): land remote sensing for global change research. IEEE Trans. Geosci. Remote Sens. 36 (4), 1228–1249.
Justice, C.O., Townshend, J.R.G., Vermote, E.F., Masuoka, E., Wolfe, R.E., Saleous, N., Roy, D.P., Morisette, J.T., 2002. An overview of MODIS land data processing and product status. Remote Sens. Environ. 83 (1–2), 3–15.
Kang, S., Kim, S., Lee, D., 2002. Spatial and temporal patterns of solar radiation based on topography and air temperature. Can. J. For. Res. 32 (3), 487–497.
Kim, J., Guo, Q., Baldocchi, D.D., Leclerc, M., Xu, L., Schmid, H.P., 2006a. Upscaling fluxes from tower to landscape: overlaying flux footprints on high-resolution (IKONOS) images of vegetation cover. Agric. Forest Meteorol. 136 (3–4), 132–146.
Kim, J., Lee, D., Hong, J.Y., Kang, S., Kim, S.J., Moon, S.K., Lim, J.H., Son, Y., Lee, J., Kim, S., Woo, N., Kim, K., Lee, B., Lee, B.L., Kim, S., 2006b. HydroKorea and CarboKorea: cross-scale studies of ecohydrology and biogeochemistry in a heterogeneous and complex forest catchment of Korea. Ecol. Res. 21 (6), 881–889.
Kjaersgaard, J.H., Plauborg, F.L., Hansen, S., 2007. Comparison of models for calculating daytime long-wave irradiance using long term data set. Agric. Forest Meteorol. 143 (1–2), 49–63.
Kustas, W.P., Norman, J.M., 2000. Evaluating the effects of subpixel heterogeneity on pixel average fluxes. Remote Sens. Environ. 74, 327–342.
Kustas, W.P., Norman, J.M., Anderson, M.C., French, A.N., 2003. Estimating subpixel surface temperatures and energy fluxes from the vegetation index–radiometric temperature relationship. Remote Sens. Environ. 85 (4), 429–440.
Lakshmi, V., Zehrfuhs, D., 2002. Normalization and comparison of surface temperatures across a range of scales. IEEE Trans. Geosci. Remote Sens. 40 (12), 2636–2646.
Lee, H.C., Hong, J., Cho, C.-H., Choi, B.-C., Oh, S.-N., Kim, J., 2003. Surface exchange of energy and carbon dioxide between the atmosphere and a farmland in Haenam, Korea. Kor. J. Agric. Forest Meteorol. 5 (2), 61–69.
Li, B., Avissar, R., 1994. The impact of spatial variability of land-surface characteristics on land-surface heat fluxes. J. Clim. 7 (4), 527–537.
Liang, S.L., 2004. Quantitative Remote Sensing of Land Surfaces. John Wiley & Sons, New Jersey.
Lim, J.H., Shin, J.H., Jin, G.Z., Chun, J.H., Oh, J.S., 2003. Forest structure, site characteristics and carbon budget of the Kwangneung Natural Foreset in Korea. Kor. J. Agric. Forest Meteorol. 5 (2), 101–109.
Liu, Y., Hiyama, T., Yamaguchi, Y., 2006. Scaling of land surface temperature using satellite data: a case examination on ASTER and MODIS products over a heterogeneous terrain area. Remote Sens. Environ. 105 (2), 115–128.
Lucht, W., Schaaf, C.B., Strahler, A.H., 2000. An algorithm for the retrieval of albedo from space using semiempirical BRDF models. IEEE Trans. Geosci. Remote Sens. 38 (2), 977–998.
Ma, Y., 2003. Remote sensing parameterization of regional net radiation over heterogeneous land surface of Tibetan Plateau and area. Int. J. Remote Sens. 24 (15), 3137–3148.
Masuoka, E., Fleig, A., Wolfe, R.E., Patt, F., 1998. Key characteristics of MODIS data products. IEEE Trans. Geosci. Remote Sens. 36 (4), 1313–1323.
Monteith, J.L., 1965. Evaporation and the environment. In: Symposium of the Society of Exploratory Biology, vol. 19. pp. 205–234.
Monteith, J.L., Unsworth, M.H., 1990. Principles of Environmental Physics. Butterworth-Heinemann Ltd., London.
Moran, M.S., Humes, K.S., Pinter Jr., P.J., 1997. The scaling characteristics of remotely sensed variables for sparsely vegetated heterogeneous landscapes. J. Hydrol. 190, 337–362.
Nishida, K., Nemani, R.R., Running, S.W., Glassy, J.M., 2003. An operational remote sensing algorithm of land surface evaporation. J. Geophys. Res. 108 (D9), 4270, doi:10.1029/2002JD002062.
Pinker, R.T., Laszlo, I., 1992. Modeling surface solar irradiance for satellite applications on a global scale. J. Appl. Meteorol. 31 (2), 194–211.
Prata, A.J., 1996. A new long-wave formula for estimating downward clear-sky radiation at the surface. Q. J. R. Meteorol. Soc. 122 (533), 1127–1151.
Priestley, C.H.B., Taylor, R.J., 1972. On the assessment of surface heat flux and evaporation using large-scale parameters. Mon. Weather Rev. 100 (2), 81–92.
Prihodko, L., Goward, S.N., 1997. Estimation of air temperature from remotely sensed surface observations. Remote Sens. Environ. 60 (3), 335–346.
Prince, S.D., Goetz, S.J., Dubayah, R.O., Czajkowski, K.P., Thawley, M., 1998. Inference of surface and air temperature, atmospheric precipitable water and vapor pressure deficit using advanced very high-resolution radiometer satellite observations: comparison with field observations. J. Hydrol. 213 (1–4), 230–249.
Pu, R., Gong, P., Michishita, R., Sasagawa, T., 2006. Assessment of multi-resolution and multi-sensor data for urban surface temperature retrieval. Remote Sens. Environ. 104 (2), 211–225.
Salomon, J.G., Schaaf, C.B., Strahler, A.H., Gao, F., Jin, Y.F., 2006. Validation of the MODIS bidirectional reflectance distribution function and albedo retrievals using combined observations from the Aqua and Terra platforms. IEEE Trans. Geosci. Remote Sens. 44 (6), 1555–1565.
Satterlund, D.R., 1979. Improved equation for estimating long-wave-radiation from the atmosphere. Water Resour. Res. 15 (6), 1649–1650.
Schaaf, C.B., Gao, F., Strahler, A.H., Lucht, W., Li, X., Tsang, T., Strugnell, N.C., Zhang, X., Jin, Y., Muller, J.-P., 2002. First operational BRDF, albedo nadir reflectance products from MODIS. Remote Sens. Environ. 83 (1–2), 135–148.
Schmid, H.P., 1997. Experimental design for flux measurements: matching scales of observations and fluxes. Agric. Forest Meteorol. 87 (2–3), 179–200.
Seemann, S.W., Li, J., Menzel, W.P., Gumley, L.E., 2003. Operational retrieval of atmospheric temperature, moisture, and ozone from MODIS infrared radiances. J. Appl. Meteorol. 42, 1072–1091.

Shuttleworth, W.J., Wallace, J.S., 1985. Evaporation from sparse crops—an energy combination theory. Q. J. R. Meteorol. Soc. 111, 839–855.

Snyder, W.C., Wan, Z.M., 1998. BRDF models to predict spectral reflectance and emissivity in the thermal infrared. IEEE Trans. Geosci. Remote Sens. 36 (1), 214–225.

Su, Z., 2002. The surface energy balance system (SEBS) for estimation of turbulent heat fluxes. Hydrol. Earth Syst. Sci. 6 (1), 85–99.

Su, H.B., McCabe, M.F., Wood, E.F., Su, Z., Prueger, J.H., 2005. Modeling evapotranspiration during SMACEX: comparing two approaches for local- and regional-scale prediction. J. Hydrometeorol. 6 (6), 910–922.

Susaki, J., Yasuoka, Y., Kajiwara, K., Honda, Y., Hara, K., 2007. Validation of MODIS albedo products of paddy fields in Japan. IEEE Trans. Geosci. Remote Sens. 45 (1), 206–217.

Swinbank, W.C., 1963. Long-wave radiation from clear skies. Q. J. R. Meteorol. Soc. 89 (381), 339–348.

Talyor, J.R., 1997. An Introduction to Error Analysis. University Science Books.

Townshend, J.R.G., Justice, C.O., 2002. Towards operational monitoring of terrestrial systems by moderate-resolution remote sensing. Remote Sens. Environ. 83 (1–2), 351–359.

Wan, Z.M., Dozier, J., 1996. A generalized split-window algorithm for retrieving land-surface temperature from space. IEEE Trans. Geosci. Remote Sens. 34 (4), 892–905.

Wan, Z., Zhang, Y., Zhang, Q., Li, Z.-l., 2002. Validation of the land-surface temperature products retrieved from Terra Moderate Resolution Imaging Spectroradiometer data. Remote Sens. Environ. 83 (1–2), 163–180.

Wan, Z., Zhang, Y., Zhang, Q., Li, Z.L., 2004. Quality assessment and validation of the MODIS global land surface temperature. Int. J. Remote Sens. 25 (1), 261–274.

Wang, K.C., Zhou, X.J., Liu, J.M., Sparrow, M., 2005. Estimating surface solar radiation over complex terrain using moderate-resolution satellite sensor data. Int. J. Remote Sens. 26 (1), 47–58.

Willmott, C.J., 1982. Some comments on the evaluation of model performance. Bull. Am. Meteorol. Soc. 63 (11), 1309–1313.

Zhang, Y.C., Rossow, W.B., Lacis, A.A., Oinas, V., Mishchenko, M.I., 2004. Calculation of radiative fluxes from the surface to top of atmosphere based on ISCCP and other global data sets: refinements of the radiative transfer model and the input data. J. Geophys. Res. 109, D19.

Zhang, J.H., Hou, Y.Y., Li, G.C., Yan, H., Yang, L.M., Yao, F.M., 2005. The diurnal and seasonal characteristics of urban heat island variation in Beijing city and surrounding areas and impact factors based on remote sensing satellite data. Sci. China Ser. D-Earth Sci. 48, 220–229.

Zillmann, J.W., 1972. A Study of Some Aspects of the Radiation and the Heat Budgets of the Southern Hemisphere Oceans, Meterological Studies, vol. 26. Bureau of Meterology, Department of the Interior, Canberra, p. 562.